Monolithic 12.5 GHz DBR- and MIR-Based Linear Extended Cavity Mode-Locked Laser in an InP Generic Foundry Platform

JIAXING DONG,[1,*] AND FRANCISCO J. DIAZ-OTERO[1,2]

[1] *University of Vigo,El Telecomunication-Campus Universitario As Lagoas,36310 Vigo,Spain*
[2] *AtlanTTic research center,El Telecomunication-Campus Universitario A sLagoas,36310 Vigo,Spain*
[*] *Jiaxing.dong@uvigo.gal*

Abstract: This paper details the development and characterization of an on-chip electrically controlled mode-locked laser (MLL) operating at 1550 nm, utilizing a generic InP foundry platform provided by HHI. Central to our study is the introduction of a novel 12 GHz MLL system with a linear laser architecture, highlighting the integration of Multimode Interference (MMI) based reflectors and Distributed Bragg Reflectors (DBRs). These components are instrumental in enhancing the MLL's performance, particularly in achieving stable mode-locking and improved spectral consistency.

Our research extensively examines the dynamics of passive mode-locking (PML) and supermode (SM) switching in this laser system. We present a detailed analysis of the interplay between key operational parameters, such as SOA current and SA voltage, and critical performance metrics like RF peak power, RF linewidth, and optical 3dB bandwidth. The study demonstrates the capability of precise tuning of these parameters to optimize the MLL's performance.

1. Introduction

Monolithic integrated mode-locked lasers (MLLs) are at the forefront of technological advancements in optoelectronics, photonics, and communication systems [1, 1]. These lasers, known for generating stable picosecond pulses, are highly valued for their compact size, high efficiency, and cost-effectiveness [2]. In particular, passive MLLs are notable for their stable mode-locking capabilities without requiring external radio-frequency (RF) modulation, which sets them apart from actively mode-locked lasers [3].

A significant aspect of our study is the focus on the advantages brought forth by the integration of active and passive components in MLL systems. This integration offers several benefits that enhance the laser's performance and versatility. Firstly, it provides the flexibility to select the total length of the cavity, which directly impacts the repetition rate [4]. This aspect is crucial for tailoring the laser's output to specific application needs. Secondly, the design reduces self-phase modulation (SPM), a common challenge in laser systems, thereby improving the quality of the laser output. The employment of Multimode Interference Reflectors (MIRs) as broadband reflectors and Distributed Bragg Reflectors (DBRs) as narrow-band but wavelength-tunable reflectors further enhances the laser's capabilities [2, 4, 5]. These components allow for precise control over the laser's spectral characteristics, making them ideal for a wide range of applications.

Thirdly, extending the cavity with an optical filter adds an additional layer of control over the bandwidth, potentially enabling harmonic mode-locking operations. Finally, the inclusion of other passive components paves the way for the effective implementation of programmable photonics circuits [6, 7]. These advancements are instrumental in pushing the boundaries of what is possible with MLL technology.

Central to this research is the exploration of wavelength sweeping facilitated by the advantageous use of MIR. The ability to precisely control and tune the wavelength is a direct consequence of the innovative design of the MLLs incorporating MIRs. This capability is pivotal for applications requiring specific wavelength operations, such as in advanced telecommunications and sensor technologies.

Our investigation into MLLs operating acrossing the whole C band, utilizing a generic InP foundry platform, aims to showcase the potential of MIR-based MLLs not only in terms of wavelength tunability but also in their ability to support multi-channel laser outputs.

2. Laser geomotery and measuremtn set up

In the device designed for this study, we introduce a novel on-chip electrically controlled MLL with a linear laser architecture, as shown in Figure 1. The laser cavity's core feature is an MMI-based reflector, providing a relatively flat reflection spectrum with a contrast of 0.4. This reflector replaces the conventional DBR approach for the left reflector, enhancing spectral consistency. Adjacent to the MMI reflector, the device integrates an E1700 (deep etched) passive waveguide, measuring 2000 μm in length. A Butt-joint (BJ) connects this passive segment to a 50 μm SOA, which acts as the Saturable Absorber (SA) in the system. Following this, a 15 μm ISO provides electrical isolation before leading to a secondary 800 μm SOA, serving as the primary gain medium. This SOA is also flanked by a 15 μm ISO, adding an extra layer of electrical insulation and supporting the MLL's smooth operation. Completing the cavity design, a 120 μm DBR with a centered wavelength of 1550 nm, suitable for typical telecom applications, is prominently placed. After this reflector, another BJ transitions to an SSC, strategically positioned at a 7° angle to minimize potential adverse reflections between the SSC and the surrounding environment. The entire laser system spans a total length of 3528μm, resulting in a foundational repetition rate of 12.5 GHz. The Device Under Test (DUT) was securely positioned on a temperature-controlled

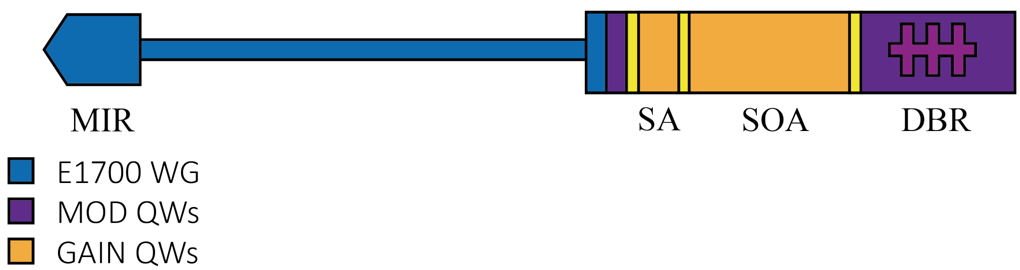

Fig. 1. Sketch of the laser cavity

copper chuck and measurements were conducted at 20 °C. A spot size converter (SSC) was utilized to assist in coupling the device to an optical fiber, significantly reducing the associated coupling losses. Notably, the SSC was strategically aligned on the chip with a 7° tilt relative to the chip edge, aiming to attenuate potential adverse effects of back reflections from the interface to the laser cavity. The emergent optical signal was proficiently detected using a THORLABS RXM40AF photoreceiver, boasting a remarkable 40 GHz bandwidth. Concurrently, the RF signal produced was accurately captured by an electrical spectrum analyzer (ESA) of type Agilent 8565EC, exhibiting a 50 GHz bandwidth. The characterization pertaining to the optical spectrum remains 0.1 GHz. For electrical interfacing, two sets of needles were connected, channeling forward current and reversed voltage to the SOA and SA, respectively.

3. 12 GHz MLL Lasing around 1550nm

The current-voltage and fiber-coupled output power characteristics (often referred to as LVI) for the MLL were measured at 20°C. As illustrated in Fig. 2.(a), the lasing threshold current is approximately 75 mA. The observed oscillations in the output power can be attributed to the shift in the wavelengths of the modes, compounded by the non-uniform gain profile of the SOA. Additionally, the map showcasing the RF peak power at the fundamental repetition rate

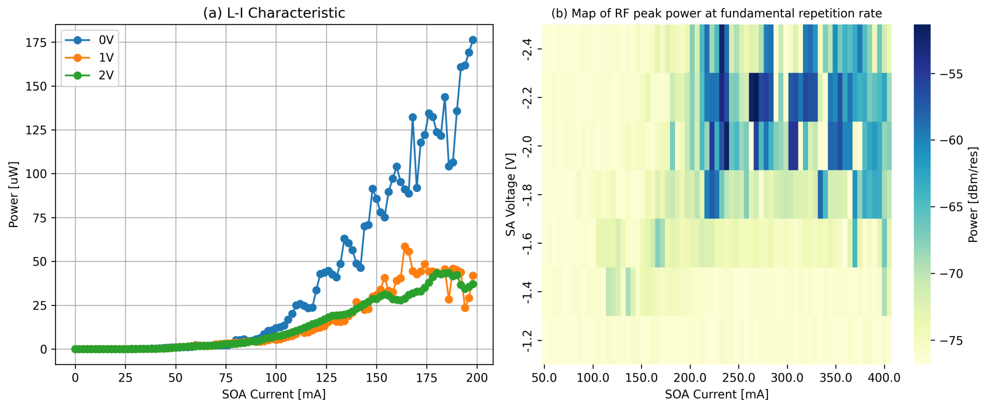

Fig. 2. (a) Optical power coupled into a lensed fiber and voltage drop across the SOA section against the injected current. (b) The map of RF peak power at the fundamental repetitial rate

was presented in Fig. 2.(b). It is evident from the data that there exists a range of operating conditions under which passive mode-locking is observed. Notably, mode-locking initiates at currents around 210 mA, and the associated SA voltage spans between -1.8V to -2.4V.

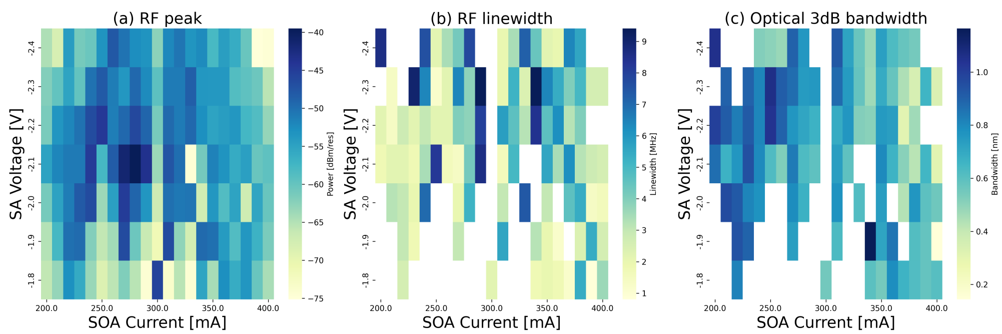

Fig. 3. (a) The map of RF peak power at the fundamental repetitial rate. (b) The map of RF linewidth at the fundamental repetitial rate. (c) The map of optical 3dB bandwidth.

A detailed investigation into the laser's performance was conducted using a finer resolution for the SOA current (10 mA) and SA voltage (0.2 V). Figure 3.(a) illustrates the RF peak power at the fundamental repetition rate (approximately 12.5 GHz) of the MLL, adjusted according to the applied working condition. It's worth noting that the background noise at this repetition rate lies between -75 to -80 dBm/res. The absence of peaks at lower frequencies indicates that the laser was not operating in the Q-switching mode. Moreover, the lower peak at the harmonic frequency compared to the fundamental repetition signifies that the laser operated in mode-locking mode, not the harmonic mode-locking mode. The RF peak observed wasn't amplified by any external amplifiers such as EDFA or SOAs. Yet, a higher RF peak could be achieved using on-chip or off-chip amplifiers. The variability in RF peak power can be attributed to differences in output power and the RF tone's linewidth at the fundamental repetition rate. Linewidth can be extensively broadened due to low-frequency noise, a phenomenon termed amplitude modulation (AM). An RF 3 dB linewidth under 10 MHz in stable mode-locking regions is depicted in Figure 3.(b).

In real-world scenarios, various noise sources, such as spontaneous emission, power source noise, cavity length variation, temperature fluctuations, and both intra-cavity and back reflections, ensure that the phase relationship among the longitudinal modes and the mode amplitudes in a mode-locked laser are not static. This noise contributes to the amplitude and timing fluctuations observed in the pulse train. Phase variation can cause the RF beat tone to broaden and induce optical pulse positional changes relative to other pulses in the sequence, a phenomenon named timing jitter. The RF spectrum also reflects amplitude jitter, which is evident in spectral components at frequencies considerably lower than the repetition rate and around the repetition rate's RF peak and its harmonics. Particularly in semiconductor mode-locked lasers, timing fluctuations influence amplitude noise and vice versa. A narrow, robust RF beat tone signal confirms the laser's efficient mode-locking behavior. The first RF harmonic's linewidth relates directly to timing jitter fluctuations [8]. One can discern a trend in Figure 3.(b) wherein the left edge of mode-locking regions consistently produces a sharp RF tone for each SOA voltage.

Figure 3.(c) maps the optical spectrum's 3 dB bandwidth, consistent with the data filter used in Figure 3.(b). Optical spectra ranged from 0.2 nm to 1.2 nm. The left edge of mode-locking regions in Figure 3.(c) indicates a trend of broader optical spectra with each SOA voltage, aligning with our earlier discussed simulation results. Pulse duration is another critical parameter; however, the laser's low output power (see Figure 2.(a)) means a typical autocorrelator would require approximately 1 W. Therefore, an amplifier (like an EDFA) becomes necessary to measure pulse duration. Regrettably, we only possess a standard EDFA; without a low-noise variant, excess noise could disrupt pulse shape, hence pulse duration characterization is absent. Assuming the output pulse is a transform-limited Gaussian pulse, the estimated output pulse width ranges from 2.94 ps to 17.6 ps. This calculation employs a time-bandwidth product factor of 0.44.

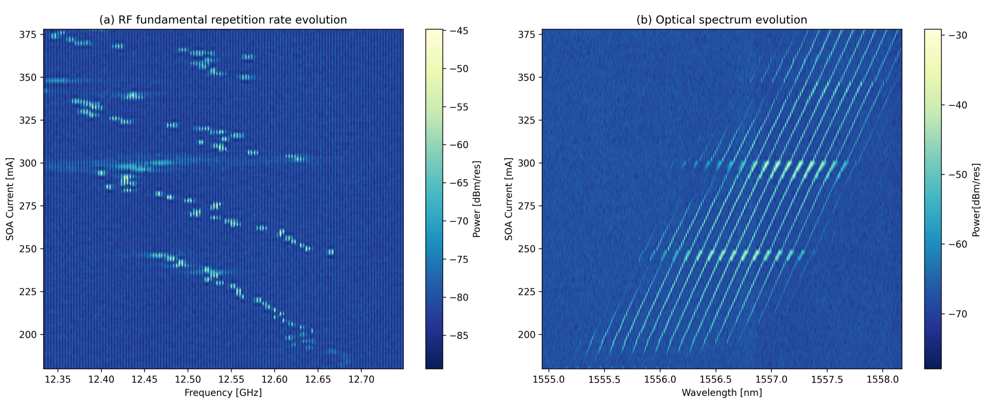

Fig. 4. (a)RF spectrum for the range of the SOA current at fixed U_{SA} = -2.2 V. (b) Optical spectrum for the range of the SOA current at fixed USA = -2.2 V.

To investigate the dynamic performance of the PMLL in more detail, a finer SOA current resolution is used (1mA). In Fig. 4.(a), we observe the evolution of the RF spectrum as a function of current with a set U_{SA} value of -2.2 V. Specifically, for currents ranging from 180 mA to 247 mA, the PML demonstrates a predominant RF tone (1st peak) that exhibits a gradual decline from 12.68 GHz to 12.45 GHz. As the SOA current increases beyond this range, a second RF peak emerges at 12.67 GHz. Between currents of 247 mA and 294 mA, the PML's fundamental RF tone (2nd peak) again sees a decline, moving from 12.66 GHz to 12.39 GHz. Analogous behavior is observed for SOA currents ranging from 305 mA to 335 mA and from 350 mA to 375 mA. Notably, within each RF tone's operational range, there exists a near-linear decrease in the RF peak corresponding to the increasing in SOA current. Fig. 4.(b) delineates the evolution of the PML's optical spectrum with respect to the injected current. The behavior exhibited in Fig. 4.(a) can be elucidated with insights from the optical spectrum. Drawing upon literature sources such as [9], we recognize that the associated frequency combs in the optical spectrum for each RF tone are termed supermodes (SM). A consistent red shift characterizes the SM within each RF tone peak range. The modulation of individual lasing modes is attributed to alterations in the refractive index, which are consequent to changes in carrier density. Notwithstanding, the varying carrier density also induces modifications to the gain curve. This explains why lasing modes on the shorter-wavelength side tend to diminish, while those on the longer-wavelength side seem to emerge with the amplifying SOA current.

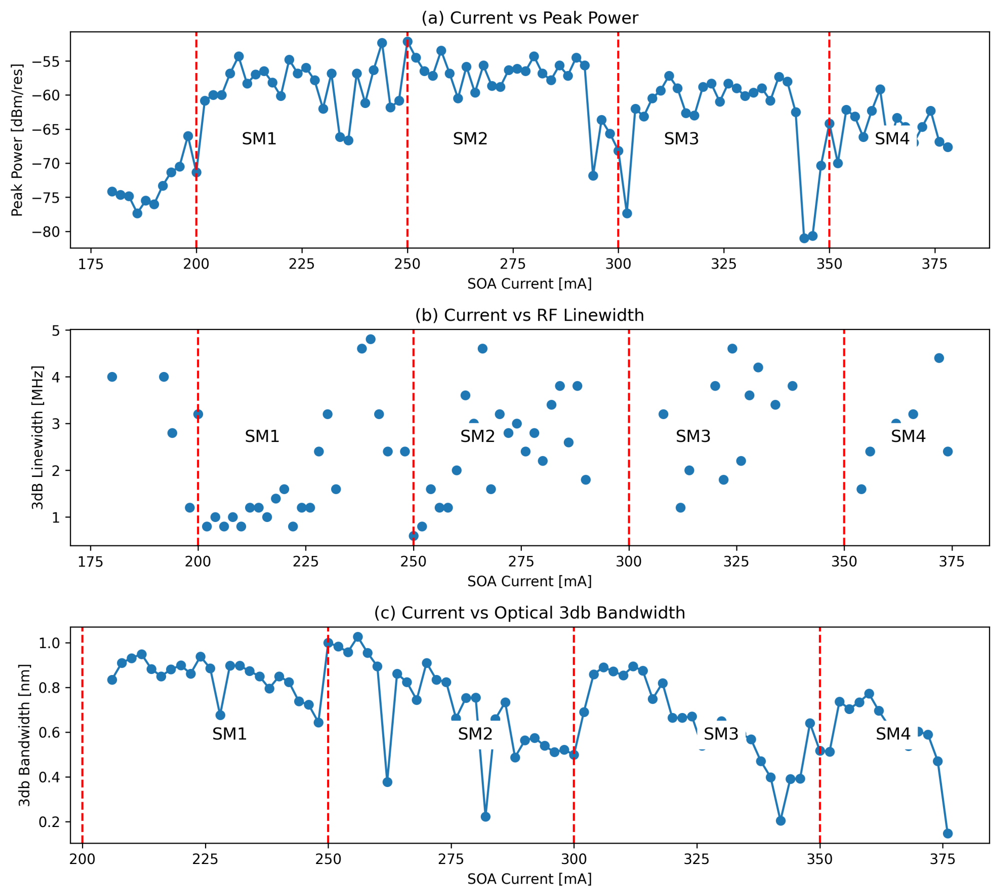

Fig. 5. (a) RF Peak power for the range of the SOA current at fixed U_{SA} = -2.2 V. (b) RF 3dB linewidth for the range of the SOA current at fixed U_{SA} = -2.2 V. (c) Optical 3dB bandwidth for the range of the SOA current at fixed U_{SA} = -2.2 V.

Figure 5.(a) illustrates the relationship between the RF peak power and the SOA current, ranging from 170 mA to 400 mA, within the four SMs regions. Within these regions, the peak power does not exhibit a discernible trend. This behavior can be attributed to several factors, including the gain and linewidth of the RF signal, as well as the range of the optical spectrum wavelength. In the context of MLL, the peak power is instrumental in determining the performance characteristics of the laser system. The absence of a clear trend in the peak power across varying SOA currents underscores the complexity of the interactions between the various contributing factors, necessitating further investigation to elucidate the underlying mechanisms.

Figure 5.(b) delineates the dependence of the RF 3dB linewidth on the SOA current in each SM region. The linewidth varies from 1 MHz at lower SOA currents to 5 MHz at higher currents, a pattern that is consistent across all four SM regions. The linewidth of the first RF harmonic is intricately related to timing jitter fluctuations [8]. Lower SOA currents correlate with reduced gain, imposing more stringent requirements on the lasing modes that contribute to ML. From this perspective, optimizing timing jitter fluctuations can be achieved by modulating the SOA current. Additionally, figure 5.(c) depicts the dependence of the optical 3dB bandwidth on the SOA current. Within each SM region, the bandwidth exhibits a decreasing trend with increasing SOA current, aligning well with the theoretical framework outlined in the preceding chapter. This observation reinforces the theoretical underpinnings discussed previously, providing empirical support for the established relationships between SOA current and optical bandwidth.

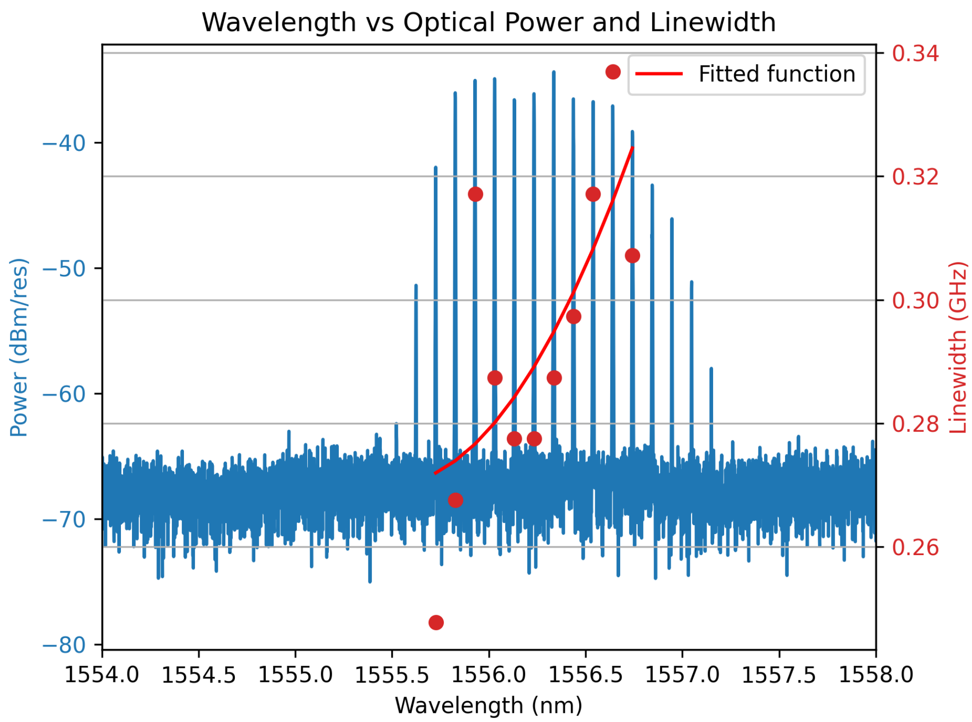

Fig. 6. Optical spectrum at I_{SOA} = 216 mA, U_{SA} = -2.2 V.

Figure 6 presents the optical spectrum measured at $I_{SOA} = 216$ mA and $U_{SA} = -2.2$ V. The linewidths of each lasing mode, denoted by red dots, range from 0.25 GHz to 0.34 GHz and are aptly fitted by a second-order parabolic curve [10]. The center of the lasing wavelength is pinpointed at approximately 1556.5 nm. This behavior can be rationalized by the unexpectedly broad bandwidth of the reflection spectrum of the DBR. Given the lower absorption characteristics of the SA at higher wavelengths, the lasing mode exhibits a propensity to operate at the higher wavelength side of the reflection spectrum of the DBR. This observation underscores the intricate interplay between the DBR's reflection spectrum and the SA's absorption properties, steering the lasing mode towards specific wavelengths and providing insights into optimizing the performance of MLL.

To investigate the dynamic performance of the PMLL in more detail, a finer SA voltage resolution is used (0.02 V). In Fig. 7.(a), we observe the evolution of the RF spectrum as a

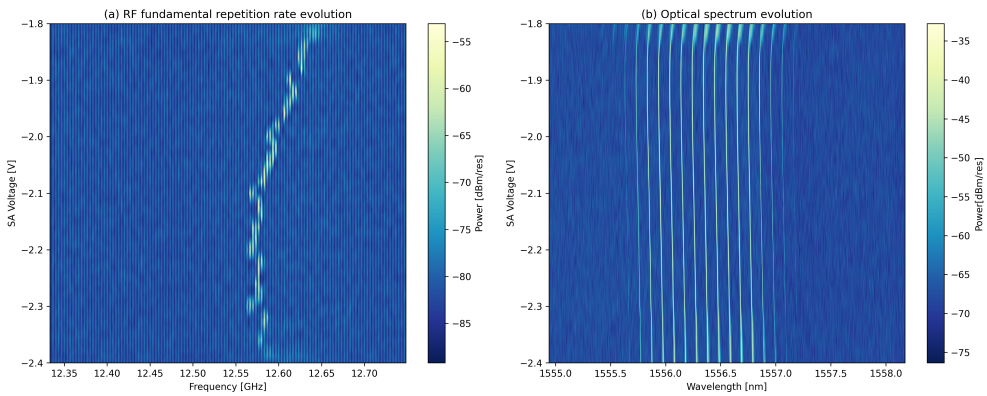

Fig. 7. (a) RF spectrum for the range of the SA voltage at fixed I_{SOA} = 220 mA. (b) Optical spectrum for the range of the SA voltage at fixed I_{SOA} = 220 mA.

function of SA voltage with a set I_{SOA} value of 220 mA. Unlike the evolution of SOA current, the RF evolution here has no jump but a increasing with the increasing the SA voltage at the begining and the trends to has a slightly decrease with the futher increasing the SA voltage from V_{SA} = -2.1V. Note the sign of the voltage is neglected here. The increasing repetition is maily caused the the QCSE effect, then the futhering increasing of the SA voltage leads to a faster recomebination, which lead to a change of the carrier density of SA and SOA at same time and this will lead the refractive change of both active components. Fig. 4.(b) delineates the evolution of the PML's optical spectrum with respect to the injected current. excpet the lasing volatge threshold aournd -1.8V, the spectrum can be considers as the same SM. the linear wavelength shift of lasing modes is due to the effective index change.

Figure 7.(a) showcases the evolution of the RF spectrum in relation to the SA voltage, with a constant I_{SOA} value of 220 mA. Contrasting with the evolution observed with varying SOA current, the RF spectrum in this scenario demonstrates no abrupt transitions. Initially, there is an increase correlating with the rising SA voltage, which subsequently tends to exhibit a slight decrement as the SA voltage continues to augment beyond $V_{SA} = -2.1$V. It is pertinent to mention that the voltage sign is disregarded in this analysis. This initial rise in the repetition rate is predominantly attributed to the QCSE. Further elevation in the SA voltage accelerates recombination, altering the carrier density in both the SA and SOA concurrently. This simultaneous shift results in modifications to the refractive indices of both active components. Subsequently, Figure 4.(b) illustrates the evolution of the PMLL's optical spectrum in response to the injected voltage. Apart from the lasing voltage threshold around -1.8V, the spectrum largely remains within the same SM. The observable linear shift in the wavelength of the lasing modes is ascribable to changes in the effective refractive index. Given that only a single SM is present in this instance, a further exploration concerning the optical spectrum bandwidth, RF 3dB linewidth, and RF peak power will not be undertaken in this discussion.

4. Conclusion

This research achieved the development of a 12 GHz mode-locked laser at 1550 nm, implemented on an InP photonic integrated circuit. Exhibiting passive mode-locking, the device demonstrated stable performance with a high signal-to-noise ratio and narrow linewidth of the fundamental beat tone. The incorporation of MMI-based reflectors and DBRs was crucial in enhancing mode-locking stability and spectral consistency. Supermode jumping, observed in the system, was analyzed and correlated with the operational conditions and characteristics of both the active and passive components.

Acknowledgments. This work has been funded by the H2020-MSCA-ITN-2019 program of the European Union under the Grant Agreement N860763 (Drive-In). The authors express their gratitude to Fraunhofer Heinrich Hertz Institute for fabricating the devices analyzed in this paper.

DISCLOSURES. Theauthorsdeclarenoconflictsofinterest.

References

1. L. Chang, S. Liu, and J. E. Bowers, "Integrated optical frequency comb technologies," Nat. Photonics **16**, 95–108 (2022).
2. P. Morton, J. Bowers, L. Koszi, *et al.*, "Monolithic hybrid mode-locked 1.3 μm semiconductor lasers," Appl. physics letters **56**, 111–113 (1990).
3. X. Huang, A. Stintz, H. Li, *et al.*, "Passive mode-locking in 1.3 μm two-section inas quantum dot lasers," Appl. Phys. Lett. **78**, 2825–2827 (2001).
4. K. Van Gasse, S. Uvin, V. Moskalenko, *et al.*, "Recent advances in the photonic integration of mode-locked laser diodes," IEEE Photonics Technol. Lett. **31**, 1870–1873 (2019).
5. R. Tucker, U. Koren, G. Raybon, *et al.*, "40 ghz active mode-locking in a 1.5 mu m monolithic extended-cavity laser," Electron. letters **10**, 621–622 (1989).
6. J. Capmany and D. Pérez, *Programmable integrated photonics* (Oxford University Press, 2020).
7. W. Bogaerts, D. Pérez, J. Capmany, *et al.*, "Programmable photonic circuits," Nature **586**, 207–216 (2020).
8. F. Kéfélian, S. O'Donoghue, M. T. Todaro, *et al.*, "Rf linewidth in monolithic passively mode-locked semiconductor laser," IEEE Photonics Technol. Lett. **20**, 1405–1407 (2008).
9. E. A. Viktorov, T. Habruseva, S. P. Hegarty, *et al.*, "Coherence and incoherence in an optical comb," Phys. review letters **112**, 224101 (2014).
10. T. Habruseva, S. O'Donoghue, N. Rebrova, *et al.*, "Optical linewidth of a passively mode-locked semiconductor laser," Opt. letters **34**, 3307–3309 (2009).